

Single-Cell Sequencing

High-Throughput Host–Microbe Single-Cell RNA Sequencing Reveals Ferroptosis-Associated Heterogeneity during *Acinetobacter baumannii* Infection

Hongen Meng⁺, Tianyu Zhang⁺, Zhang Wang⁺, Yuyi Zhu, Yingying Yu, Hangfei Chen, Jiaye Chen, Fudi Wang, Yunsong Yu, Xiaoting Hua,* and Yongcheng Wang*

Abstract: Interactions between host and bacterial cells are integral to human physiology. The complexity of host–microbe interactions extends to different cell types, spatial aspects, and phenotypic heterogeneity, requiring high-resolution approaches to capture their full complexity. The latest breakthroughs in single-cell RNA sequencing (scRNA-seq) have opened up a new era of studies in host–pathogen interactions. Here, we first report a high-throughput cross-species dual scRNA-seq technology by using random primers to simultaneously capture both eukaryotic and bacterial RNAs (scRandom-seq). Using reference cells, scRandom-seq can detect individual eukaryotic and bacterial cells with high throughput and high specificity. *Acinetobacter baumannii* (*A.b*) is a highly opportunistic and nosocomial pathogen that displays resistance to many antibiotics, posing a significant threat to human health, calling for discoveries and treatment. In the *A.b* infection model, scRandom-seq witnessed polarization of THP-1 derived-macrophages and the intracellular *A.b*-induced ferroptosis-stress in host cells. The inhibition of ferroptosis by Ferrostatin-1 (Fer-1) resulted in the improvement of cell vitality and resistance to *A.b* infection, indicating the potential to resist related infections. scRandom-seq provides a high-throughput cross-species dual single-cell RNA profiling tool that will facilitate future discoveries in unraveling the complex interactions of host–microbe interactions in infection systems and tumor micro-environments.

Introduction

Interactions between host and bacterial cells are crucial for human physiology, with bacteria adapting to the host micro-environment and the immune system distinguishing beneficial bacteria from pathogens. The outcome of host–pathogen encounters depends not only on bacterial virulence traits but also on the timing, location, and manner of interaction with host cells.^[1–5] The complexity of host–microbe interactions extends to different cell types, spatial aspects, and phenotypic heterogeneity, requiring high-resolution approaches to capture their full complexity at various scales, from the whole organism to individual cells.^[4–5] *Acinetobacter baumannii* (*A.b*) is a Gram-negative bacterium and a highly opportunistic pathogen that poses a significant threat to human health, particularly in clinical settings where antibiotic-resistant strains are prevalent.^[6] Infecting the human host requires a coordinated response from *A.b* that not only impairs cellular defense mechanisms, mainly in the form of protection via the capsular polysaccharide, but also enables metabolic and nutritional flexibility.^[6–7] Recently, a growing body of research has focused on understanding the mechanisms of *A.b* infection and the host–microbe interactions.^[7–9] Studying *A.b* infection at the single cell level may offer novel insights and opportunities for developing innovative treatments to combat *A.b* infections, given its rapid acquisition of multidrug, extensive drug, and even pan drug resistance phenotypes.

The latest breakthroughs in scRNA-seq have opened up a new era of transcriptomics, leading to significant discoveries of previously unknown cell types, physiological states, and principles of stochastic gene expression. The 10X Genomics Chromium scRNA-seq platform has been widely

[*] Dr. H. Meng,⁺ T. Zhang,⁺ J. Chen, Prof. Y. Wang
 Department of Laboratory Medicine of The First Affiliated Hospital & Liangzhu Laboratory, Zhejiang University School of Medicine, Hangzhou 310030, China
 E-mail: yongcheng@zju.edu.cn

Dr. Z. Wang,⁺ Dr. H. Chen, Prof. Y. Yu, Prof. X. Hua
 Department of Infectious Diseases, Sir Run Run Shaw Hospital, Zhejiang University School of Medicine, Hangzhou 310016, People's Republic of China
 E-mail: xiaotinghua@zju.edu.cn

Y. Zhu
 M20 Genomics, Hangzhou, 311121, China

Dr. Y. Yu, Prof. F. Wang
 The Second Affiliated Hospital, School of Public Health, Zhejiang University School of Medicine, Hangzhou 310016, China

Prof. Y. Yu, Prof. X. Hua
 Key Laboratory of Microbial Technology and Bioinformatics of Zhejiang Province, Hangzhou 310016, China

Prof. Y. Yu, Prof. X. Hua
 Regional Medical Center for National Institute of Respiratory Diseases, Sir Run Run Shaw Hospital, School of Medicine, Zhejiang University, Hangzhou 310016, China

[†] These authors contributed equally to this work.

used on eukaryotes.^[10] A prevalent constraint encountered in eukaryotic scRNA-seq methodologies, including but not limited to 10X Genomics Chromium, and BD Rhapsody,^[11] is their reliance on oligo(dT)-primed reverse transcription (RT) to capture poly(A)⁺ RNAs. This reliance results in the omission of information pertaining to numerous non-polyadenylated RNA categories, most notably small eukaryotic RNAs.

Recently, our group developed droplet-based single-cell RNA sequencing technologies for FFPE tissues^[12] and bacteria,^[13] with state-of-art high-throughput, high-sensitivity, and high-coverage, by capturing full-length total RNAs with random primers, in accordance with prior studies,^[14–15] showing that random primer-based RT exhibited enhanced efficiency and a broader capacity for capturing both eukaryotic and prokaryotic RNAs. In addition, other groups have developed PETRI-seq,^[15] microSPLiT,^[16] and BacDrop^[17] for bacterial scRNA-seq. The primary goal of scRNA-seq in host–microbe systems goes beyond the capabilities of dual RNA-seq as it aims to simultaneously profile and correlate gene expression changes in both individual infected host cells and the microbes.^[18–19] Because of the highly abundant host cell RNA and permeabilization differences between cells and bacteria, such bacterial scRNA-seq technologies^[13,15–17] cannot be used directly to study complex host–microbe systems. Although scDual-Seq^[20] based on CEL-Seq2^[21] method is a single cell dual RNA-seq method that could capture both host and bacterial transcriptomes, it necessitates cell sorting and in vitro reactions in a single well for each cell which have disadvantages of complicated operation and far from reaching high-throughput level. However, dual scRNA-seq is still in its early stages.

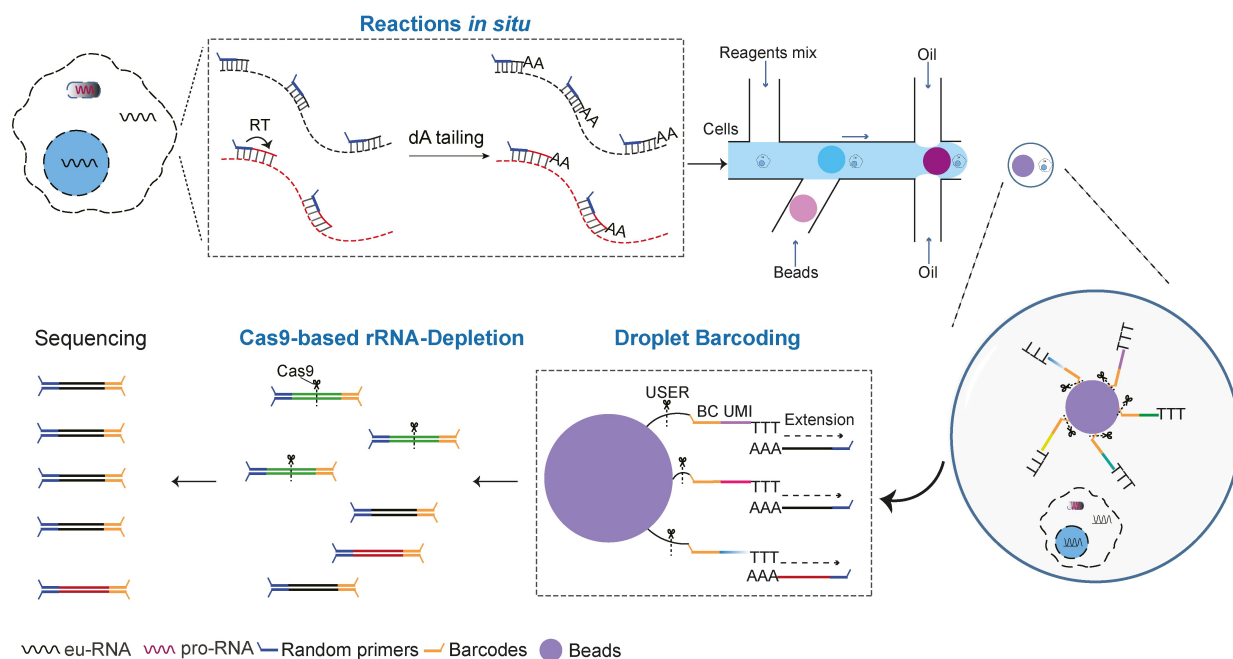
In this study, based on our newly developed random-primer-based scRNA-seq chemistry,^[12–13] we reported a droplet-based, high-throughput host–microbe scRNA-seq (scRandom-seq) to simultaneously capture eukaryotic and prokaryotic RNA and try to investigate the mechanisms and interactions between host and pathogenic microbes at the single cell level. Compared with existing technologies,^[12,13] scRandom-seq has several improvements in adopting appropriate permeabilization, pre-index strategy introducing, barcoding equipment optimization, host rRNA-depletion, and a new pipeline for host–microbe single cell analysis. Our scRandom-seq demonstrated high sensitivity and quantitative in mixed eukaryotic and prokaryotic samples, and identified polarization of host cells and the inhibition of ferroptosis on resistance to *A.b* in THP-1 derived macrophages (M ϕ) (THP-1 M ϕ) model infected by *A.b*. Our scRandom-seq approach will enable us to investigate the interactions and underlying mechanisms between individual host cells and bacteria at higher throughput and finer resolution, with implications for the host–microbe interactions and related samples.

Results and Discussion

The workflow of our scRandom-seq method in host–microbe related samples is schematically shown in Figure 1. To make our scRandom-seq applicable to multiple species samples, we optimized the protocol for fixing and permeabilizing the host cells and microbes to maintain RNA integrity,^[13–14,16–17] adopted random primers-based reverse transcription (RT) reaction capturing of total RNAs and dA-tailing which enables second strand synthesis using oligo-dT primers. The RT primers consist of random primers which contain mainly G, A and T bases and have a high affinity for binding both eukaryotic and prokaryotic RNA which results in high efficiency of RT,^[12,22–23] and a pre-indexing sequence that enables us to load each droplet with multiple cells and minimize genetic contamination.^[24] Then droplet barcoding was conducted on our customized automated droplet microfluidics platform following a previously described protocol,^[25,26] which is suitable for capturing both individual host cells and bacteria (Figure S1A). The hydrogel barcoded beads were developed based on previous studies^[25,26] and synthesized utilizing a 3-step ligation reaction (Figure S1B). In droplets, cell barcoding was achieved via second-strand cDNA synthesis. To enrich the mRNA portion of the sequencing investment, Cas9-based rRNA-depletion was employed which could significantly reduce the portion of rRNA in sequencing data.^[27–29] Further, a new pipeline for host–microbe single cell analysis was developed, mainly consisting of cross-species genome alignment and integrated analysis of host and microbial gene expression patterns. Considering the permeabilization effect on the eukaryotic cells with lysozyme, we found the gene expression pattern of the THP-1 M ϕ treated with lysozyme did not change ($R=0.95$, $p<2.2e-16$) (Figure S1C–E).

Then, the technical performance of scRandom-seq was evaluated using reference cells. First, we conducted a standard eukaryotic species-mixing experiment with a mixture of 293T cells (Human) and 3T3 cells (Mouse) with scRandom-seq. Of the 6083 cells which had high-quality and unique barcodes (the ROGUE values (purity, reads percentage of the corresponding annotation taxon)^[30] were both >0.96 (Figure S2A)), 2860 (47.0%) and 3136 (51.6%) cells were aligned to Human and Mouse respectively (median genes reached to 2392 and 2213 for Human and Mouse clusters (Figure S2B)), while only 1.4% contained reads mapped to both species (Figure 2a), indicating a low cross barcode contamination rate in our method. All biotypes of eukaryotic RNA were captured, including mRNA, lncRNA, rRNA, miRNA, snoRNA, snRNA, misc_RNA, etc. (Figure S2C). Unlike most poly(A)-based scRNA-seq platforms with obvious 3'-end bias, scRandom-seq displayed evenly distributed coverage from 3' to 5'-end of the gene body (Figure S2D). Additionally, saturation analysis showed that the number of genes detected in scRandom-seq had not reached saturation point by 50 k uniquely aligned reads per 3T3 and 293T cells (Figure S1E). Then, to further demonstrate the benchmark of scRandom-seq for prokaryotic species, we tested it on an *A.b*, *Escherichia coli* (*E.coli*) and *Klebsiella pneumoniae* (*K.p*) mixture (AEK mixture). The

scRandom-seq workflow



Host-microbe single cell analysis

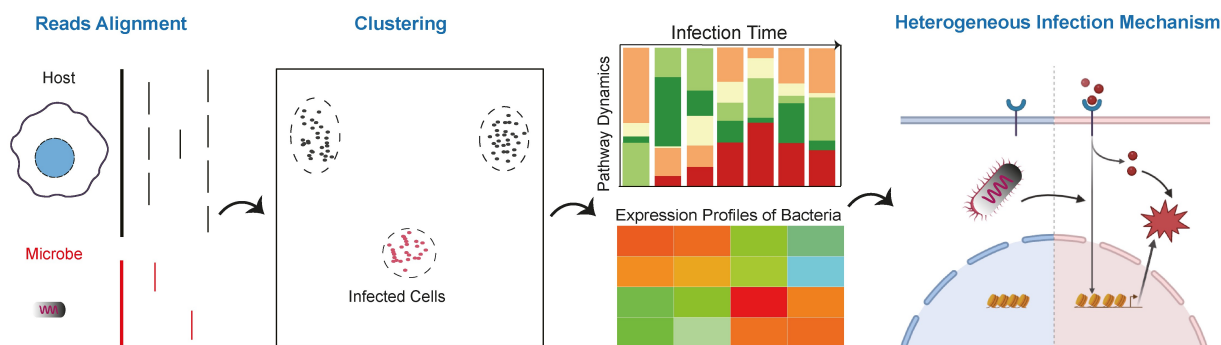


Figure 1. Schematic diagram of the scRandom-seq method on infection model.

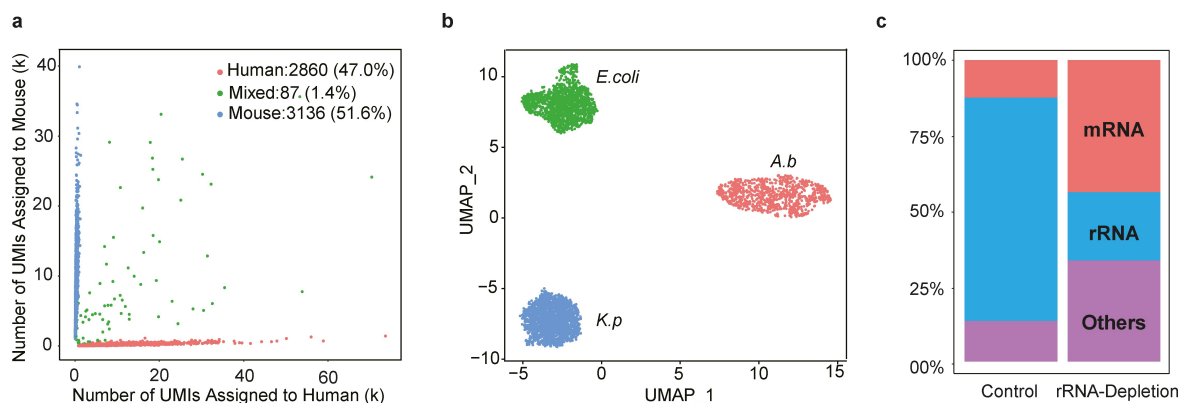


Figure 2. a, Scatter plot of Human and Mouse UMI counts per cell barcode in a mixture of 293T and 3T3 sample. Identified 293T: $n=2875$, identified 3T3: $n=3289$. b, Scatter plot of *A.b*, *E.coli*, and *K.p* UMI counts per cell barcode in a mixture of *A.b*, *E.coli*, and *K.p* sample. Identified *A.b*: $n=839$; identified *E.coli*: $n=1140$; identified *K.p*: $n=1800$. c, Representative proportions of transcript categories of control and rRNA-depleted THP-1 Mø sample. *A.b*: *Acinetobacter baumannii*, *E.coli*: *Escherichia coli*, *K.p*: *Klebsiella pneumoniae*; THP-1 Mø, THP-1 derived macrophages (Mø).

generated sequencing data sets demonstrated similar alignment visualizations through UMAP dimensionality reduction, resulting in clear separation (Figure 2b). The purity analysis revealed that the majority of barcodes exhibited high species purity (>95%) (Figure S2F). Our scRandom-seq technique effectively captured RNA from each bacterial species, with a median count of over 200 genes per cell for *A. b* (274), *E. coli* (249), and *K. p* (221) (Figure S2G).

To test the efficiency of Cas9-based rRNA depletion, we designed 114 guide RNAs (gRNA) according to the human rDNA sequences under the optimized experimental conditions as described in the method section.^[27] The rRNA proportion reduced from 73.5% to 22.4%, while the coding base was increased almost four times (12% to 44%) (Figure 2c) without changing the gene expression pattern (Figure S2H). Overall, we showed that scRandom-seq worked well both in eukaryotic and prokaryotic samples.

To further validate scRandom-seq in simultaneously capturing both host and pathogen transcriptomes at single cell level, we used the intracellular-bacteria models in which the THP-1 M ϕ were infected with *A. b* at a 50:1 MOI (Multiplicity of Infection) for two time points (0.5 h and 4.0 h) (Figure 3a). The infected samples were washed with PBS, treated with gentamicin to kill extracellular bacteria, and then washed again. Along with the uninfected THP-1 M ϕ samples, we processed all three samples with the following steps: 1) perform lysis and the CFU (Colony Forming Unit) assay to count the number of intracellular bacteria (Figure S3A and Figure S3B); 2) implement the scRandom-seq procedures (the median UMI of the three samples reached to about 2000 (Figure S3C)). The CFU assay showed that the CFU was 0 ± 0 (mean \pm SEM) at 0 h, 8000 ± 2000 (mean \pm SEM) at 0.5 h, and 16000 ± 1000 (mean \pm SEM) at 4.0 h (Figure S3A and Figure S3B), indicating the *A. b* internalization of the infected samples. To ensure the accuracy of the detection, we set up negative controls during the experimental process, not only for uninfected samples but also for environmental negative samples. In the process of data analysis, threshold lines are set based on the sequencing results of the two negative controls mentioned above to ensure the authenticity of the obtained sequencing data. By performing the scRandom-seq and unbiased comparison of THP-1 derived M ϕ and *A. b* reads across the three time points using Seurat, we found that the three samples showed four expression patterns (cluster 1 for the uninfected samples (821 cells), cluster 0 for the 0.5 h-infected samples (944 cells), and cluster 2 (423 cells) and cluster 3 (156 cells) for the 4.0 h-infected samples) (Figure 3b). The detected *A. b* reads in the three samples showed a similar increasing trend with the CFU assay from 0 h to 4.0 h (Figure 3c and Figure S3D). The gene counts per cell and total gene counts of *A. b* detected from the uninfected and the two time points infected samples were shown in Figure S3E and Table S1, the transcripts of bacteria in infected samples are 10 times or more than those in uninfected samples similar transcript expression trends observed in scDual-Seq,^[20] but scRandom-seq has high-throughput advantages that scDual-Seq does not have. Although the number of reads of *A. b* per host cell was

low when averaged, it is sufficient to conduct relevant analyses if combining all *A. b* reads in each cluster (Table S1 and Table S2). Although some single-cell RNA-seq studies have detected several bacteria RNA,^[31] bacterial total RNA cannot be covered. The reason for the fewer detected reads of intracellular *A. b* in single host cells is that the bacterial cells contain only a femtogram amount of RNA, that is, >100 times less than the typical eukaryotic cell.^[5] Currently, we look at bulk bacterial gene expression within eukaryotic host cell clusters. Further efforts are needed to optimize the current technologies for looking at bacterial expression at the single host cell in dual host–bacterium RNA-seq experiments, such as optimizing the permeabilization and reverse transcription to improve the capture efficiency of bacterial transcripts, and selectively enriching bacterial reads by bacterial DNA target enrichment probes or reducing non-coding transcripts of both host and bacterium by Cas9-based depletion.

We termed cluster 0 THP-1 M ϕ as the “early infection cells” for three reasons: 1) their global transcriptional patterns were more similar to the uninfected than other infected cells; 2) the number of intracellular bacteria was lower than other infected cells; 3) highly variable genes in cluster 0 (CCDC91 and SPART) showed phagosome-related features (Figure S4A). We termed cells in cluster 2 and cluster 3 as the “late infection cells” as their highly variable genes (such as PTGS2, CCL3L3, TRAF1, and TNF) were enriched in immune activation-related pathways (Figure 3d and Table S3). Combined highly differential expressed genes (DEGs) (the average of \log_2 Foldchange >0.6, the adjusted-*p* value <0.05) enriched in infection-related pathways such as *Salmonella* infection, TNF signaling pathway, IL-17 signaling pathway, Ferroptosis, NF-kappa B signaling pathway, Apoptosis, NOD-like receptor signaling pathway, Toll-like receptor signaling, Necroptosis, Phagosome, etc. (Figure 3e and Figure S4B), which represented the response of host cells at different stages of infection. For PTGS2, flow cytometry analysis in the uninfected THP-1 M ϕ samples and infected THP-1 M ϕ samples showed enhanced protein levels in the infected samples (Figure S5A), which supported our finding in cluster 2 and cluster 3. Through our scRandom-seq, polarization has been observed in *A. b* infected THP-1 M ϕ during infection as in various single-cell studies.^[32–33]

Moreover, the reprogramming trajectory in a pseudo-temporal manner using Monocle 3^[34] (Figure 3f) among the cells in Figure 3b showed that the expression patterns represented the infection processes just as the time-points of infection manner from the uninfected cells (cluster 1) to the “early infection cells” (cluster 0) and the “late infection cells” (cluster 2 and cluster 3). Though some cells did not engulf *A. b*, they still exhibited similar expression patterns to those of infected cells at the same time, which might be caused by cell-cell communications.^[33]

Although the cells in cluster 2 and cluster 3 all came from the 4.0 h time-point samples and were sorted together in our pseudo-temporal analysis, they did have different expression patterns, as shown in Figure 3b. Therefore, we did further the KEGG enrichment analysis using their specific DEGs to identify the differences between them. As

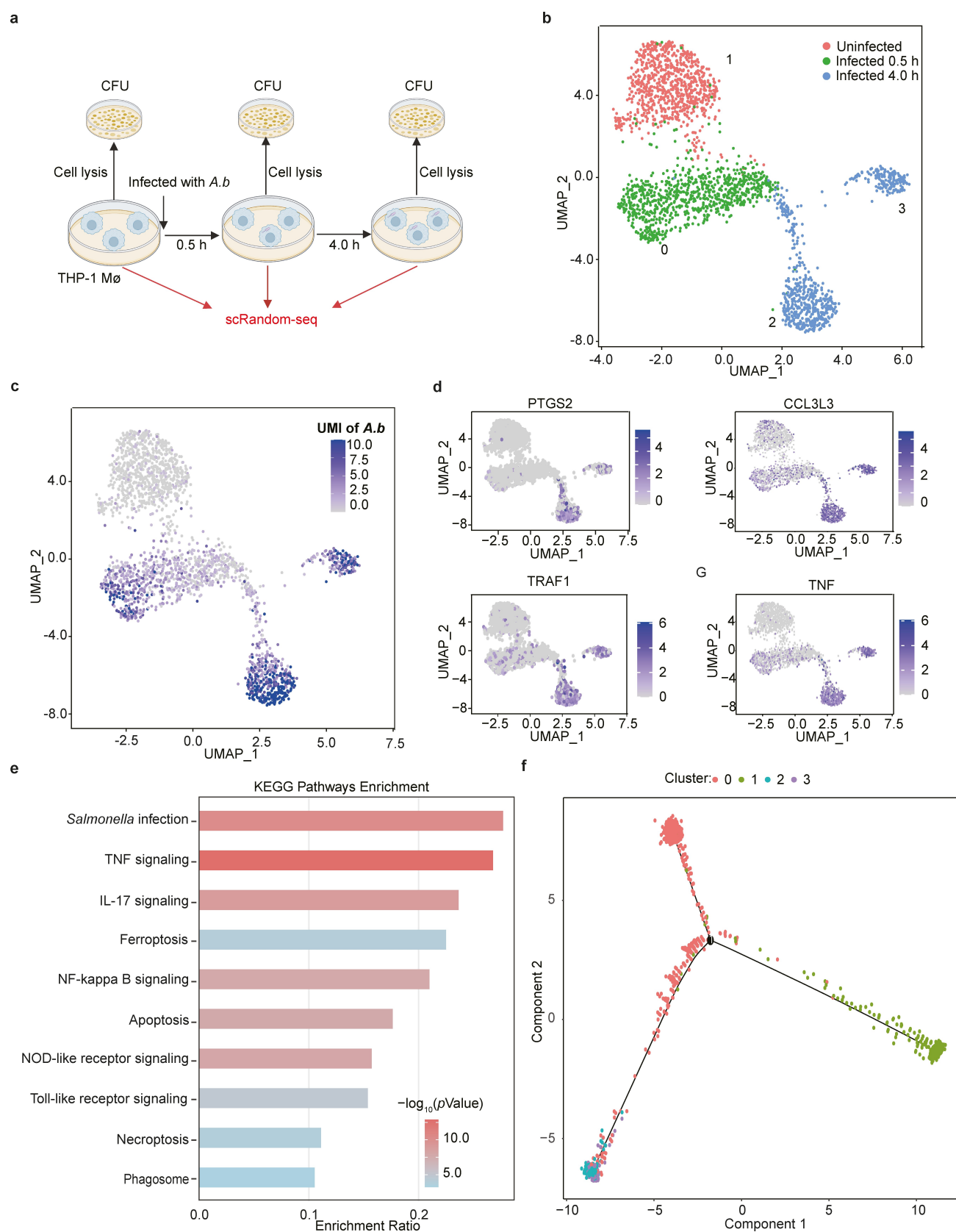


Figure 3. scRandom-seq showed the THP-1 M ϕ polarization depending on *A. b* infection **a**, THP-1 M ϕ , exposed or unexposed to *A. b*, were collected and processed with CFU assay or using scRandom-seq at the three time-points. **b**, UMAP projection of all the cells collected at the different time points, based on their gene expression colored by time-point. **c**, The detected reads of intracellular *A. b* in the tested cells. **d**, Top Differential expressed genes (DEGs) among cluster 2 and cluster 3. **e**, Histogram of KEGG enrichment analysis of top DEGs in cluster 0, 1, 2 and 3. **f**, The reprogramming trajectory colored by the pseudo-time order of the cells using Monocle 3.

shown in Figure S4B, the TNF signaling pathway, NF-kappa B signaling pathway, *Salmonella* infection, IL-17 signaling pathway, Toll-like receptor signaling, NOD-like receptor signaling, Apoptosis, and Necroptosis were highly ranked both in cluster 2 and cluster 3, and all these pathways belonged to the host's innate immune responses. Interestingly, we found that Ferroptosis pathway and HIF-1 signaling were more prominent in cluster 2 than in cluster 3 (Figure 4a). Ferroptosis is a newly defined programmed cell death characterized by iron overload and lipid peroxidation, which was also found in *Pseudomonas aeruginosa*, *Mycobacterium tuberculosis*, *Magnaporthe oryzae*, *S.aureus*, and *E.coli* infection.^[35–39] The ferroptosis-related gene TFRC, SLC39A14, ACSL1, HMOX1(HO-1), ACSL5, and NCOA4 were among the top DEGs in cluster 2 when compared to

cluster 3 and cluster 1 (the uninfected samples) (Figure 4b and Figure S4C).

Highly expressed TFRC and SLC39A14 in cluster 2 might transport the Fe^{3+} and Fe^{2+} into the cytoplasm respectively, while HMOX1 catalyzed heme degradation and facilitated the release of free iron,^[40] which all resulted in Fe^{2+} accumulation in the cytoplasm and the subsequent aggravated Fenton reaction accompanied with the ferritinophagy degradation by NCOA4.^[41] The increased PUFA-CoA caused by the upregulation of ACSL1 and ACSL5 and the increased Fenton reaction together led to lipid peroxidation and, ultimately, ferroptosis in host cells.^[42,43]

We assumed the ferroptosis-stress in cluster 2 cells other than cluster 3 cells could be attributed to the different expression patterns of the intracellular *A.b* in the host cells. So we combined all *A.b* reads in each cluster for conducting

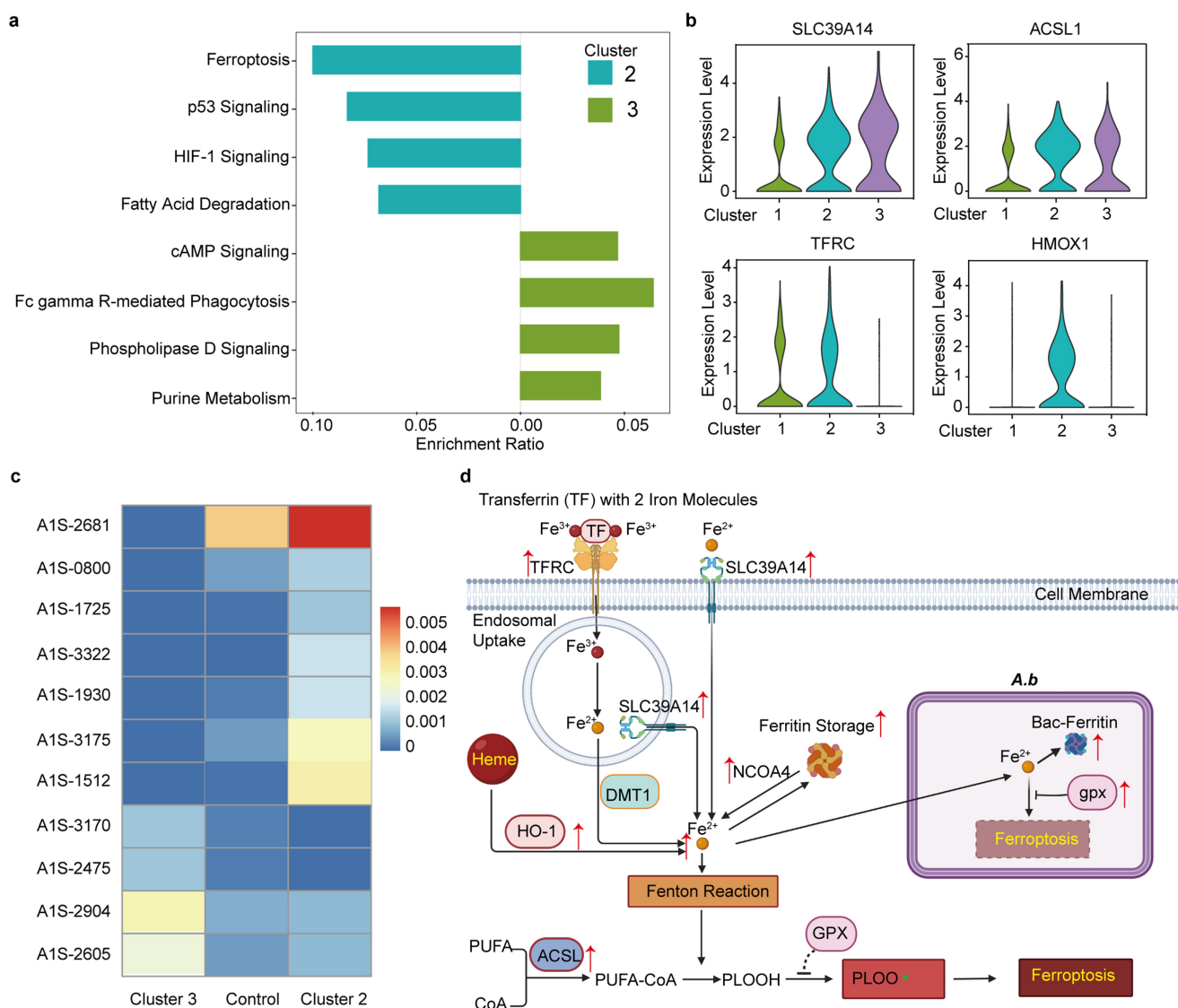


Figure 4. Host–microbe heterogeneity was driven by Ferroptosis-stress induced by intracellular *A.b* a, Histogram of KEGG enrichment analysis of top DEGs in cluster 2 and 3 separately. b, Expression of genes involved in Ferroptosis pathway in sub-clusters. c, Expression of genes of intracellular *A.b* involved in bacterioferritin and cell division. d, The diagram of ferroptosis-stress and expression of related genes in the cells and intracellular *A.b* in cluster 2 cells. HO-1: HMOX1

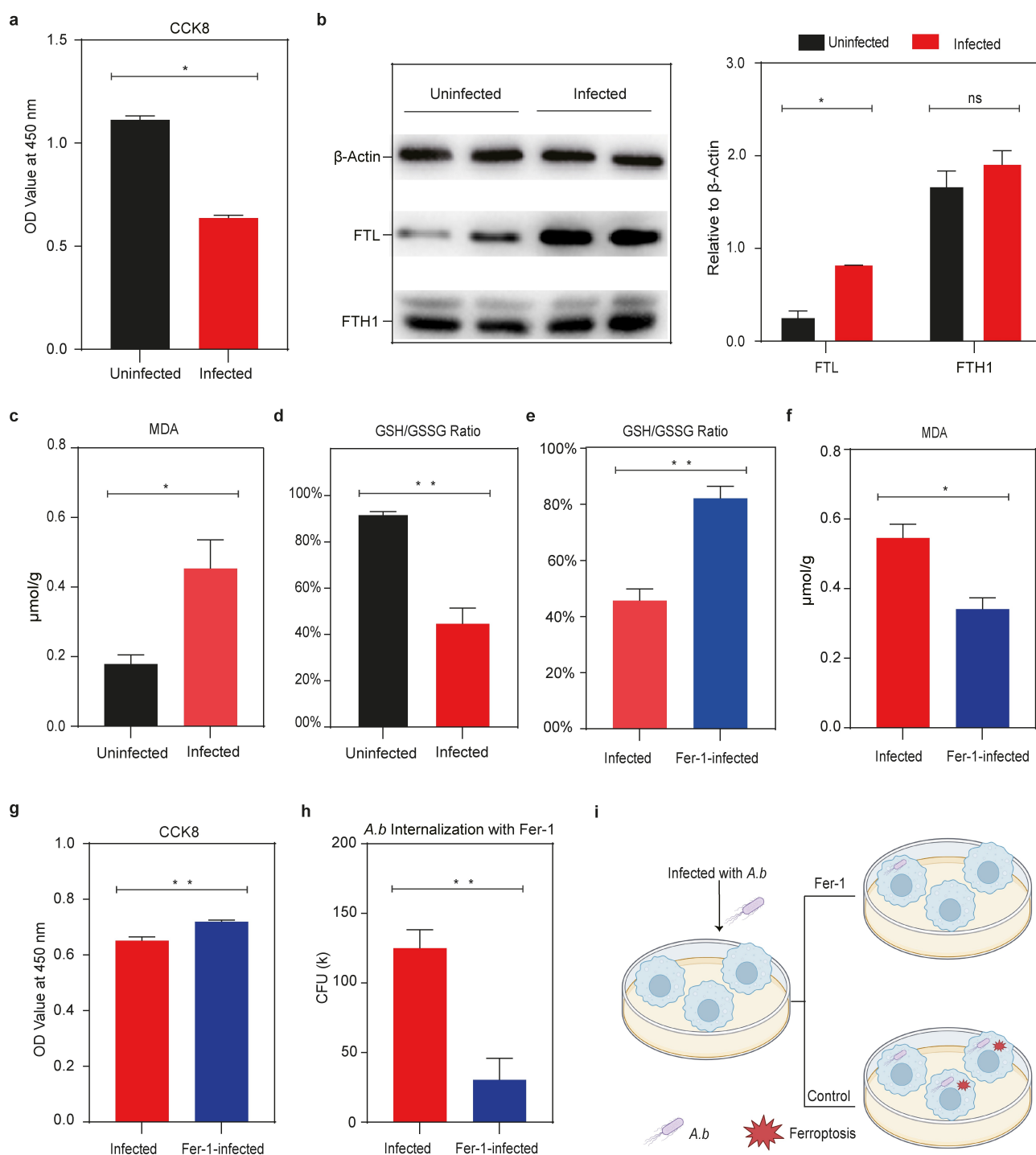


Figure 5. Inhibiting ferroptosis by Ferrostatin-1 helped host cells to resist *A.b* infection **a**, The OD value at 450 of the uninfected THP-1 Mø samples and the 4.0 h-infected samples in CCK8 assay. **b**, western blot and the relative FTL and FTH1 level of the uninfected THP-1 Mø samples and the 4.0 h-infected samples. **c**, MDA of the uninfected THP-1 Mø samples and the 4.0 h-infected samples. **d**, GSH/GSSG ratio of the uninfected THP-1 Mø samples and the 4.0 h-infected samples. **e**, GSH/GSSG ratio of the 4.0 h-infected samples and Ferrostatin-1 (Fer-1) treated 4.0 h-infected samples. **f**, MDA of the 4.0 h-infected samples and Fer-1 treated 4.0 h-infected samples. **g**, The OD value at 450 of the 4.0 h-infected samples and Fer-1 treated 4.0 h-infected samples in CCK8 assay. **h**, The *A.b* internalization of the 4.0 h-infected samples and Fer-1 treated 4.0 h-infected samples. **i**, Schematic diagram of Fer-1 on resisting *A.b* infection. ns: not significantly; *: $0.01 < p < 0.05$; **: $0.001 < p < 0.01$.

relevant analyses, and the total detected *A.b* genes in cluster 0, 1, 2, and 3 were shown in Table S1, which was sufficient to conduct the relevance analysis. Specifically, the

average gene expression level for each cluster was calculated by the total UMI count of each *A.b* genes within the cluster divided by the total UMI of intracellular *A.b* in each cluster.

For control samples, the average gene expression level was calculated by the total UMI count of each *A.b* genes/total UMI of all *A.b* cells in the three bacteria mixed sample. Surprisingly, the expression patterns of intracellular *A.b* in the cluster 2 and cluster 3 cells were completely different (Table S4). The genes of intracellular *A.b* in the cluster 2 cells which encode bacterioferritin (A1S-0800 and A1S-3175), ferredoxin (A1S-1512 and A1S-3322), ferric siderophore receptor protein (A1S-1725), and cell division protein (A1S-2681 and A1S-1930) were highly expressed (Figure 4c and Figure S5B), suggesting that the intracellular *A.b* was in a state of cell division with a higher demand for iron, which can explain the reason of iron accumulation trend in the cytoplasm of host cells. Unlike the host cells in cluster 2, the glutathione peroxidase (gpx, a ferroptosis inhibitor^[44]) in the intracellular *A.b* in cluster 2 cells was significantly up-regulated, which might inhibit the occurrence of ferroptosis and facilitate cell survival and replication. Therefore, we proposed the following diagram to show how the demand for iron of intracellular *A.b* drives the ferroptosis-stress in the host cells to survive and even replicate in vivo (Figure 4d): The intracellular *A.b* might be in the stage of differentiation and appreciation, exhibiting a high demand for iron, leading to a significant accumulation of iron in the host cells.^[1,45,46] This process is mediated by the up-regulation of TFRC, SLC39A14, and HMOX1, ultimately leading to a significant increase in iron-mediated Fenton reaction in the cytoplasm. Specifically, TFRC and SLC39A14 could promote iron absorption by cells, and some studies have shown that SLC39A14 and TFRC are induced by TNF- α .^[32–33,47] HMOX1 catalyzes heme to release Fe²⁺, and as a target gene of the HIF-1 pathway that was found activated in cluster 2, it would be expressed during infection for some bacteria to create a hypoxic environment which would activate the HIF pathway in host cells.^[2,40] These two processes ultimately lead to a significant increase of the iron-mediated Fenton reaction in the cytoplasm. At the same time, the up-regulation of ACSL1/5, as the inducer of ferroptosis,^[42–43] would promote the production of a large amount of PUFA-CoA, which, in conjunction with the abundant free radicals generated by the Fenton reaction, lead to lipid peroxidation and the accompanying ferroptosis-stress. By overexpressing GPX, the key ferroptosis-inhibiting factor,^[46] intracellular bacteria could survive and even grow or proliferate without ferroptosis stress.

To verify our hypothesis in Figure 4d whether ferroptosis occurred and benefited the host cells or the bacteria, the biomarkers (FTL and FTH1 for intracellular iron, glutathione to oxidized glutathione (GSH/GSSG) ratio and MDA for oxidative stress) were tested and the inhibitor Ferrostatin-1 (Fer-1) was used. We found that the activity of THP-1 M ϕ infected for 4.0 h was indeed severely inhibited through Cell Counting Kit-8 (CCK8) assay for cell proliferation and cytotoxicity test (Figure 5a). Meanwhile, compared with uninfected cells, the expression of FTL was significantly increased (Figure 5b), and the uncropped blot images were in Figure S6), suggesting a significant accumulation of iron in host cells. The significant decrease in GSH/GSSG ratio (Figure 5c) and the significant increase in MDA

content (Figure 5d) both indicated an increase of lipid peroxidation in host cells. Based on these results, there was indeed a pressure of ferroptosis within the host cells. Next, we experimented on ferroptosis inhibition mediated by Fer-1. The GSH/GSSG ratio and MDA of THP-1 M ϕ cells treated with 10 μ M Fer-1 were significantly reversed (Figure 5e and 5f), indicating that the pressure of ferroptosis was suppressed. Correspondingly, the cell viability of the host cells was significantly improved (Figure 5g and Figure S7A), and the CFU experiment of the cell lysis after infection confirmed a significant decrease in the internalized *A.b* (Figure 5h, Figure S7B, and S7C). Unlike the study stated that ferroptosis stress promoted macrophages against intracellular bacteria,^[39] we assumed that intracellular *A.b* was the cause of ferroptosis-stress in the host cells, leading to a decrease in cell viability, like the ferroptosis triggered in bronchial epithelium cells by *Pseudomonas aeruginosa*^[35] and *Mycobacterium tuberculosis* infection.^[36] The introduction of Fer-1 can substantially alleviate the burden of ferroptosis, consequently enhancing cell viability and, ultimately, bolstering resistance against bacterial infections. So, alleviating the ferroptosis stress of host cells could effectively resist *A.b* infection and might become a therapeutic target. In summary, inhibiting ferroptosis in host cells could prevent *A.b* invasion of host cells (Figure 5i).

Conclusion

In conclusion, we demonstrated scRandom-seq, a new high-throughput host–microbe dual scRNA-seq technology, and evaluated its detection efficacy in eukaryotic samples and different bacteria samples. Applying this technology to the *A.b* infection model, we witnessed the ferroptosis-associated heterogeneity in host cells for the first time, which suggests that ferroptosis may become a new clinical target for resisting *A.b* infection. The application of this advanced scRNA-seq technology holds promising prospects in various fields, particularly in the context of human tumors, where bacteria function can impact cancer patient outcomes.^[48–51] The colonization and proliferation play a role in regulating immune function and impacting cancer patient outcomes.^[48–51] The scRandom-seq opens up exciting possibilities for investigating host–microbe interactions in infection models and tumor–microbe samples which could aid understanding of disease progression and treatment strategies.

Data and Code Availability

The RNA sequencing data are available at the Genome Sequence Archive (GSA) under the BioProject accession number HRA004751 and CRA011250. This paper does not report original code. Any additional information required to reanalyze the data reported in this work is available from the lead contact upon request.

Acknowledgements

The project was supported by the National Natural Science Foundation of China (No. 32200073 and 32250710678, Y.W.), Leading Innovative and Entrepreneur Team Introduction Program of Zhejiang (No.2021R01012, Y.W.), and “Pioneer” R&D programs of Zhejiang Province (No. 2024C03005, Y.W.). We thank the core facilities of Liangzhu Laboratory and Zhejiang University School of Medicine for their excellent technical support. Parts of the Figures were created using BioRender.com.

Conflict of Interest

Y.W. is a co-founder, and Y.Z. is an employee of M20 Genomics. The other authors declare no conflict of interest.

Data Availability Statement

The data that support the findings of this study are available from the corresponding author upon reasonable request.

Keywords: Single cell RNA-seq · Droplet microfluidics · Host–microbe interactions · *Acinetobacter baumannii* infection · Ferroptosis

- [1] L. Diacovich, J. P. Gorvel, *Nat. Rev. Microbiol.* **2010**, *8*(2), 117–128.
- [2] A. C. André, M. Laborde, B. S. Marteyn, *Trends Microbiol.* **2022**, *30*(7), 643–653.
- [3] I. Jorgensen, M. Rayamajhi, E. A. Miao, *Nat. Rev. Immunol.* **2017**, *17*(3), 151–164.
- [4] D. G. Russell, L. Huang, B. C. VanderVen, *Nat. Rev. Immunol.* **2019**, *19*(5), 291–304.
- [5] A. J. Westermann, J. Vogel, *Nat. Rev. Genet.* **2021**, *22*(6), 361–378.
- [6] C. M. Harding, S. W. Hennon, M. F. Feldman, *Nat. Rev. Microbiol.* **2018**, *16*(2), 91–102.
- [7] W. Zhang, Y. Yao, H. Zhou, J. He, J. Wang, L. Li, M. Gao, X. Liu, Y. Shi, J. Lin, J. Liu, H. Chen, Y. Feng, Z. Zhou, Y. Yu, X. Hua, *Emerging microbes & infections* **2022**, *11*(1), 2556–2569.
- [8] P. Gallagher, S. Baker, *J. Infect.* **2020**, *81*(6), 857–861.
- [9] E. R. Green, J. N. Fakhoury, A. J. Monteith, H. Pi, D. P. Giedroc, E. P. Skaar, *Cell Host Microbe* **2022**, *30*(7), 975–987.e7.
- [10] G. X. Zheng, J. M. Terry, P. Belgrader, P. Ryvkin, Z. W. Bent, R. Wilson, S. B. Ziraldo, T. D. Wheeler, G. P. McDermott, J. Zhu, M. T. Gregory, J. Shuga, L. Montesclaros, J. G. Underwood, D. A. Masquelier, S. Y. Nishimura, M. Schnell-Levin, P. W. Wyatt, C. M. Hindson, R. Bharadwaj, A. Wong, K. D. Ness, L. W. Beppu, H. J. Deeg, C. McFarland, K. R. Loeb, W. J. Valente, N. G. Ericson, E. A. Stevens, J. P. Radich, T. S. Mikkelsen, B. J. Hindson, J. H. Bielas, *Nat. Commun.* **2017**, *8*, 14049.
- [11] H. C. Fan, G. K. Fu, S. P. Fodor, *Science* **2015**, *347*(6222), 1258367.
- [12] Z. Xu, T. Zhang, H. Chen, Y. Zhu, Y. Lv, S. Zhang, J. Chen, H. Chen, L. Yang, W. Jiang, S. Ni, F. Lu, Z. Wang, H. Yang, L. Dong, F. Chen, H. Zhang, Y. Chen, J. Liu, D. Zhang, L. Fan, G. Guo, Y. Wang, *Nat. Commun.* **2023**, *14*(1), 2734.
- [13] Z. Xu, Y. Wang, K. Sheng, R. Rosenthal, N. Liu, X. Hua, T. Zhang, J. Chen, M. Song, Y. Lv, S. Zhang, Y. Huang, Z. Wang, T. Cao, Y. Shen, Y. Jiang, Y. Yu, Y. Chen, G. Guo, P. Yin, D. A. Weitz, Y. Wang, *Nat. Commun.* **2023**, *14*(1), 5130.
- [14] Y. Fu, H. Chen, L. Liu, Y. Huang, *Anal. Chem.* **2016**, *88*(22), 10795–10799.
- [15] S. B. Blattman, W. Jiang, P. Oikonomou, S. Tavazoie, *Nature microbiology* **2020**, *5*(10), 1192–1201.
- [16] A. Kuchina, L. M. Brettner, L. Paleologu, C. M. Roco, A. B. Rosenberg, A. Carignano, R. Kibler, M. Hirano, R. W. DePaolo, G. Seelig, *Science* **2021**, *371*(6531), eaba5257.
- [17] P. Ma, H. M. Amemiya, L. L. He, S. J. Gandhi, R. Nicol, R. P. Bhattacharyya, C. S. Smillie, D. T. Hung, *Cell* **2023**, *186*(4), 877–891.e14.
- [18] A. J. Westermann, K. U. Förstner, F. Amman, L. Barquist, Y. Chao, L. N. Schulte, L. Müller, R. Reinhardt, P. F. Stadler, J. Vogel, *Nature* **2016**, *529*(7587), 496–501.
- [19] D. A. C. Stapels, P. W. S. Hill, A. J. Westermann, R. A. Fisher, T. L. Thurston, A. E. Saliba, I. Blommestein, J. Vogel, S. Helaine, *Science* **2018**, *362*(6419), 1156–1160.
- [20] T. Hashimshony, N. Senderovich, G. Avital, A. Klochendler, Y. de Leeuw, L. Anavy, D. Gennert, S. Li, K. J. Livak, O. Rozenblatt-Rosen, Y. Dor, A. Regev, I. Yanai, *Genome Biol.* **2016**, *17*, 77.
- [21] G. Avital, R. Avraham, A. Fan, T. Hashimshony, D. T. Hung, I. Yanai, *Genome Biology* **2017**, *18*(1), 200.
- [22] K. Sheng, W. Cao, Y. Niu, Q. Deng, C. Zong, *Nat. Methods* **2017**, *14*(3), 267–270.
- [23] F. Imdahl, E. Vafadarnejad, C. Homberger, A. E. Saliba, J. Vogel, *Nature microbiology* **2020**, *5*(10), 1202–1206.
- [24] P. Datlinger, A. F. Rendeiro, T. Boenke, M. Senekowitsch, T. Krausgruber, D. Barreca, C. Bock, *Nat. Methods* **2021**, *18*(6), 635–642.
- [25] Y. Wang, T. Cao, J. Ko, Y. Shen, W. Zong, K. Sheng, W. Cao, S. Sun, L. Cai, Y. L. Zhou, X. X. Zhang, C. Zong, R. Weissleder, D. Weitz, *Adv. Sci.* **2020**, *7*(8), 1903463.
- [26] J. Ko, Y. Wang, K. Sheng, D. A. Weitz, R. Weissleder, *ACS Nano* **2021**, *15*(3), 5631–5638.
- [27] W. Gu, E. D. Crawford, B. D. O’Donovan, M. R. Wilson, E. D. Chow, H. Retallack, J. L. DeRisi, *Genome Biology* **2016**, *17*, 41.
- [28] G. Prezza, T. Heckel, S. Dietrich, C. Homberger, A. J. Westermann, J. Vogel, *RNA* **2020**, *26*(8), 1069–1078.
- [29] C. Homberger, R. J. Hayward, L. Barquist, J. Vogel, *mBio* **2023**, *14*(2), e0355722.
- [30] B. Liu, C. Li, Z. Li, D. Wang, X. Ren, Z. Zhang, *Nat. Commun.* **2020**, *11*(1), 3155.
- [31] A. E. Saliba, L. Li, A. J. Westermann, S. Appenzeller, D. A. Stapels, L. N. Schulte, S. Helaine, J. Vogel, *Nature microbiology* **2016**, *2*, 16206–2501.
- [32] M. Nanami, T. Ookawara, Y. Otaki, K. Ito, R. Moriguchi, K. Miyagawa, Y. Hasuike, M. Izumi, H. Eguchi, K. Suzuki, T. Nakanishi, *Arterioscler. Thromb. Vasc. Biol.* **2005**, *25*(12), 2495–501.
- [33] A. Sayadi, A. T. Nguyen, F. A. Bard, E. A. Bard-Chapeau, *Inflammation Res.* **2013**, *62*(2), 133–143.
- [34] X. Qiu, Q. Mao, Y. Tang, L. Wang, R. Chawla, H. A. Pliner, C. Trapnell, *Nat. Methods* **2017**, *14*(10), 979–982.
- [35] H. H. Dar, Y. Y. Tyurina, K. Mikulska-Ruminska, I. Shrivastava, H. C. Ting, V. A. Tyurin, J. Krieger, C. M. St Croix, S. Watkins, E. Bayir, G. Mao, C. R. Armbruster, A. Kapralov, H. Wang, M. R. Parsek, T. S. Anthony-muthu, A. F. Ogunsola, B. A. Flitter, C. J. Freedman, J. R. Gaston, T. R. Holman, J. M. Pilewski, J. S. Greenberger, R. K. Mallampalli, Y. Doi, J. S. Lee, I. Bahar, J. M. Bomberger, H. Bayir, V. E. Kagan, *J. Clin. Invest.* **2018**, *128*(10), 4639–4653.

- [36] E. P. Amaral, D. L. Costa, S. Namasivayam, N. Riteau, O. Kamenyeva, L. Mittereder, K. D. Mayer-Barber, B. B. Andrade, A. Sher, *J. Exp. Med.* **2019**, *216*(3), 556–570.
- [37] N. Millet, N. V. Solis, D. Aguilar, M. S. Lionakis, R. T. Wheeler, N. Jendzjowsky, M. Swidrigall, *Nat. Commun.* **2022**, *13*(1), 5545.
- [38] S. Dangol, Y. Chen, B. K. Hwang, N. S. Jwa, *Plant Cell* **2019**, *31*(1), 189–209.
- [39] R. Ma, L. Fang, L. Chen, X. Wang, J. Jiang, L. Gao, *Theranostics* **2022**, *12*(5), 2266–2289.
- [40] X. Fang, H. Wang, D. Han, E. Xie, X. Yang, J. Wei, S. Gu, F. Gao, N. Zhu, X. Yin, Q. Cheng, P. Zhang, W. Dai, J. Chen, F. Yang, H. T. Yang, A. Linkermann, W. Gu, J. Min, F. Wang, *Proc. Natl. Acad. Sci. USA* **2019**, *116*(7), 2672–2680.
- [41] J. D. Mancias, X. Wang, S. P. Gygi, J. W. Harper, A. C. Kimmelman, *Nature* **2014**, *509*(7498), 105–109.
- [42] Q. Zhang, L. Xiong, T. Wei, Q. Liu, L. Yan, J. Chen, L. Dai, L. Shi, W. Zhang, J. Yang, S. Roessler, L. Liu, *Oncogene* **2023**, *42*(19), 1509–1523.
- [43] A. Beatty, T. Singh, Y. Y. Tyurina, V. A. Tyurin, S. Samovich, E. Nicolas, K. Maslar, Y. Zhou, K. Q. Cai, Y. Tan, S. Doll, M. Conrad, A. Subramanian, H. Bayir, V. E. Kagan, U. Rennefahrt, J. R. Peterson, *Nat. Commun.* **2021**, *12*(1), 2244.
- [44] M. Huang, Z. Wang, L. Yao, L. Zhang, X. Gou, H. Mo, H. Li, L. Hu, X. Zhou, *Int. J. Antimicrob. Agents* **2023**, *61*(5), 106794.
- [45] M. Nairz, U. Schleicher, A. Schroll, T. Sonnweber, I. Theurl, S. Ludwiczek, H. Talasz, G. Brandacher, P. L. Moser, M. U. Muckenthaler, F. C. Fang, C. Bogdan, G. Weiss, *J. Exp. Med.* **2013**, *210*(5), 855–873.
- [46] J. Mayneris-Perxachs, J. M. Moreno-Navarrete, J. M. Fernández-Real, *Nat. Rev. Endocrinol.* **2022**, *18*(11), 683–698.
- [47] G. Wang, A. K. Biswas, W. Ma, M. Kandpal, C. Coker, P. M. Grandgenett, M. A. Hollingsworth, R. Jain, K. Tanji, S. López-Pintado, A. Borczuk, D. Hebert, S. Jenkitkasemwong, S. Hojyo, R. V. Davuluri, M. D. Knutson, T. Fukada, S. Acharyya, *Nat. Med.* **2018**, *24*(6), 770–781.
- [48] B. Ghaddar, A. Biswas, C. Harris, M. B. Omary, D. R. Carpizo, M. J. Blaser, S. De, *Cancer Cell* **2022**, *40*(10), 1240–1253.e5.
- [49] D. Nejman, I. Livyatan, G. Fuks, N. Gavert, Y. Zwing, L. T. Geller, A. Rotter-Maskowitz, R. Weiser, G. Mallel, E. Gigi, A. Meltzer, G. M. Douglas, I. Kamer, V. Gopalakrishnan, T. Dadosh, S. Levin-Zaidman, S. Avnet, T. Atlan, Z. A. Cooper, R. Arora, A. P. Cogdill, M. A. W. Khan, G. Ologun, Y. Bussi, A. Weinberger, M. Lotan-Pompan, O. Golani, G. Perry, M. Rokah, K. Bahar-Shany, E. A. Rozeman, C. U. Blank, A. Ronai, R. Shaoul, A. Amit, T. Dorfman, R. Kremer, Z. R. Cohen, S. Harnof, T. Siegal, E. Yehuda-Shnaidman, E. N. Gal-Yam, H. Shapira, N. Baldini, M. G. I. Langille, A. Ben-Nun, B. Kaufman, A. Nissan, T. Golan, M. Dadiani, K. Levanon, J. Bar, S. Yust-Katz, I. Barshack, D. S. Peeper, D. J. Raz, E. Segal, J. A. Wargo, J. Sandbank, N. Shental, R. Straussman, *Science* **2020**, *368*(6494), 973–980.
- [50] A. Fu, B. Yao, T. Dong, Y. Chen, J. Yao, Y. Liu, H. Li, H. Bai, X. Liu, Y. Zhang, C. Wang, Y. Guo, N. Li, S. Cai, *Cell* **2022**, *185*(8), 1356–1372.e26.
- [51] E. Riquelme, Y. Zhang, L. Zhang, M. Montiel, M. Zoltan, W. Dong, P. Quesada, I. Sahin, V. Chandra, A. San Lucas, P. Scheet, H. Xu, S. M. Hanash, L. Feng, J. K. Burks, K. A. Do, C. B. Peterson, D. Nejman, C. D. Tzeng, M. P. Kim, C. L. Sears, N. Ajami, J. Petrosino, L. D. Wood, A. Maitra, R. Straussman, M. Katz, J. R. White, R. Jenq, J. Wargo, F. McAllister, *Cell* **2019**, *178*(4), 795–806.e12.

Manuscript received: January 8, 2024

Accepted manuscript online: February 28, 2024

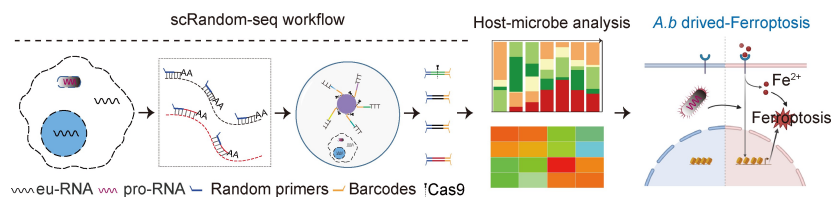
Version of record online: ■■■, ■■■

Research Articles

Single-Cell Sequencing

H. Meng, T. Zhang, Z. Wang, Y. Zhu, Y. Yu,
H. Chen, J. Chen, F. Wang, Y. Yu, X. Hua,*
Y. Wang* **e202400538**

High-Throughput Host–Microbe Single-Cell RNA Sequencing Reveals Ferroptosis-Associated Heterogeneity during *Acinetobacter baumannii* Infection



We demonstrated scRandom-seq, a new high-throughput Random primer-based host–microbe dual single-cell RNA sequencing technology, and applied this technology to an *Acinetobacter baumannii* (*A.b*) infection model. We witnessed

the ferroptosis-associated heterogeneity in host cells for the first time, which suggests that ferroptosis may become a new clinical target for resisting *A.b* infection.